TEM and molecular simulation studies on the hydroxylapatite structure with Si and Mg impurities

M. E. FERNÁNDEZ[1], C. ANGELES-CHAVEZ[2], G. MONDRAGÓN-GALICIA[1], V. RODRÍGUEZ-LUGO[3,4*]
[1]*Instituto Nacional de Investigaciones Nucleares, km 36.5 Carretera México-Toluce, Ocoyoacac Edo, de México C.P. 52045, México*
[2]*Instituto Mexicano del Petróleo, Programa de Ingeniería Molecular, Eje Central Lázaro Cárdenas 152, 07730 México D.F.*
[3]*Centro Universitario de Vinculación, Benemérita Universidad Autónoma de Puebla 29 Oriente 601-1 Col. Ladrillera de Benítez Puebla, Puebla México, C.P. 72540*
[4]*Facultad de Ingeniería Química, Benemérita Universidad Autónoma de Puebla Avenida San Claudio y 18 sur, Ciudad Universitaria, C.P. 72570 Puebla, México*
E-mail: lugo.ventura@cuv.buap.mx

Transmission electron microscopy (TEM) and molecular simulation studies of traces of chemical elements such as Mg, Si, and OH in the hydroxylapatite (CaHAP) crystal structure obtained from the sand dollar were carried out. Two different types of CaHAP crystal morphologies in the samples synthesized by the hydrothermal method used were observed. Reflections with regular intensity in the experimental electron diffraction patterns obtained from these morphologies were observed. However, when these results were compared with a simulated electron diffraction pattern (which was obtained using the crystalline structure proposed for the hydroxylapatite) some forbidden reflections in the experimental pattern were observed. Then, in order to reproduce the experimental patterns Si and Mg atoms in the crystalline lattice were introduced. These elements in the elemental chemical analysis carried out by X-ray energy dispersive spectroscopy (EDS) in the typical CaHAP morphologies were detected. The positions of these atoms in the asymmetric unit were obtained using molecular simulation and during the relaxation process, the structure did not show changes in the lattice parameters. Subsequently, the crystalline structure was reproduced and matched the electron diffraction patterns simulated resulting in the experimental electron diffraction pattern. Experimental and simulated X-ray diffraction spectra were also matched.

Introduction

The study of hydroxylapatite has increased during the last decades, because it is the main mineral that constitutes the tissues of bone and teeth. Also, this material receives special attention due to the different mechanisms that have an impact on the synthesis process [1–4]. These different mechanisms define the characteristics of the final product such as morphology, particle size, homogenous chemical composition, and crystal structure [5]. Also, it is important to mention that the synthesized CaHAP is of interest in bioceramics since it can be used as an adsorbent for biomaterials and as an ion exchanger, chemical sensor, and catalyst [6]. However, the physiochemical properties of this compound depend strongly on crystal stoichiometry and in the surface state [7]. For example, biogenic hydroxylapatite is often associated with a variety of trace constituents such as Mg^{2+} [8, 9], Na^{+}, CO_3^{2-}, Cl^{-} [10], $Sr2^{+}$ [11], F^{-} [12] and $P_2O_7^{4-}$ [13]. Therefore, these materials are structurally and compositionally complex. Some of these ions can enter into the crystal lattice while others are only adsorbed at surface levels.

The presence of extraneous ions may also play an important role in determining the nucleation process, crystal growth, morphology, aggregation, ion exchange, adsorption, and dissolution properties of biological and synthetic hydroxylapatite [14]. Inorganic ions such as Cl^{-} [15], F^{-} [16], CO_3^{2-} [17] Li^{+} [18] and Sr^{2+} [19] have been shown to produce morphological effects. This is not surprising, since the morphology of CaHAP can be

*Author to whom all correspondence should be addressed.

TABLE I Composition of the samples

Sample	CaO (g)	$CaHPO_4$ (g)	Temperature (°C)	Pressure (MPa)	Time (h)
HCa20651	1.0	3.63	270	6.5	20
HCaO201	0.5	1.0	270	6.5	20
HCa20652	1.0	1.0	270	6.5	20
HCaO202	1.5	1.0	270	6.5	20
HCaO203	2.0	1.0	270	6.5	20
HCaO204	2.5	1.0	270	6.5	20

significantly different in contrasting biological tissues such as bone (plate-like) and enamel (needle-like) hexagonal prism. Furthermore, many of the properties of synthetic CaHAP will be influenced by crystal size, shape and surface area, which could be relevant to the use of CaHAP in chromatography, catalysis and ion exchange, orthopedics, and dentistry [14]. Therefore, to investigate the positions of the extraneous atoms into the crystalline lattice will allow determination of the specific application of synthetic hydroxylapatite. In this work, we present a study of the extraneous atoms within the crystalline CaHAP structure. These CaHAP crystals were obtained from the sand dollar, which has a small amount of Si and Mg. Their presence into the CaHAP structure has an effect on the diffraction phenomena, which has been studied by transmission electron microscopy (TEM) and molecular simulation.

Experimental procedure

Samples with different calcium oxide compositions were prepared to produce CaHAP crystals. Table I shows the chemical compositions of each sample. Sand dollar and monetite ($CaHPO_4$) were used as sources of CaO and PO_4^{-3} ions, respectively. The synthesis was carried out through a hydrothermal method, using a Monel autoclave. The reaction was sustained at 6.5 Mpa of pressure, 270 °C of temperature for 20 h.

The structural and chemical characterization of single CaHAP crystals obtained in each sample was carried out in a JEM 2010 transmission electron microscope, which has attached to it an energy dispersive spectrometer. In order to analyze the material, the samples were deposited on a copper grid cover with a thin polymeric film and carbon. The samples were previously dispersed in isopropilic alcohol by ultrasonic agitation.

Simulation procedure

The hydroxylapatite model with impurities was built using the program Cerius2 that allows the geometric optimization of the hydroxylapatite model with impurities by quantum mechanical simulation. The calculus is based on the density functional theory (DFT) that uses the local density approximation (LDA) and the generalized gradient approximation (GGA) developed by Perdew and Wang [20]. Simulated images were obtained by the multislice method [21] using the atomic position [22]. The transmission electron microscope parameters used to carry out the simulation process correspond to the JEOL 2010 microscope. This has the following characteristics: an accelerating voltage of 200 keV, a spherical aberration coefficient of 1.2 mm, a beam divergence half-angle of 0.6 mrad, and a Scherzer resolution of 0.17 nm. These parameters are similar to the JEM 2010 microscope used to obtain the experimental data.

Results and discussion

A detailed description of the microstructural and chemical characterization of the product reaction was reported in a previous work [23] and the study of the hydroxylapatite crystals obtained by the hydrothermal method used is now presented.

Two different morphology types of CaHAP crystals were observed. Fig. 1(a) shows the typical fiber shape of CaHAP crystals and Fig. 1(b) shows CaHAP crystals with hexagonal plane shape. Electron diffraction pattern were obtained from these morphologies and their analysis show that the fiber grew along the *c*-axis (Fig. 2(a)) while the CaHAP crystal with hexagonal plane

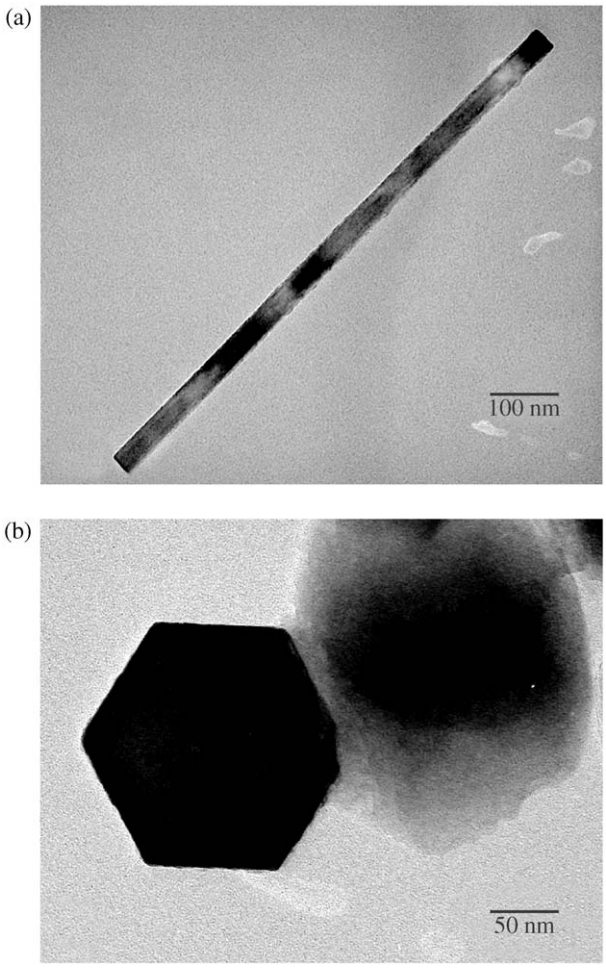

Figure 1 Typical morphologies of the hydroxylapatite crystals (a) fiber and (b) hexagonal plane shape.

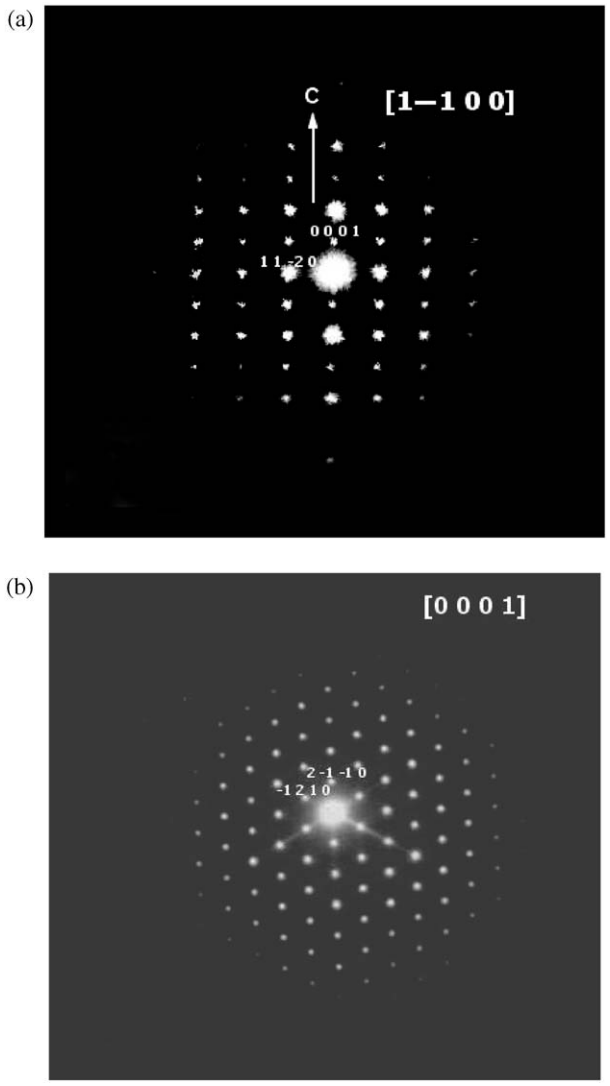

Figure 2 Electron diffraction pattern obtained from the morphologies of the hydroxylapatite crystals (a) $[1\,-1\,0\,0]$ and (b) $[0\,0\,0\,1]$ directions.

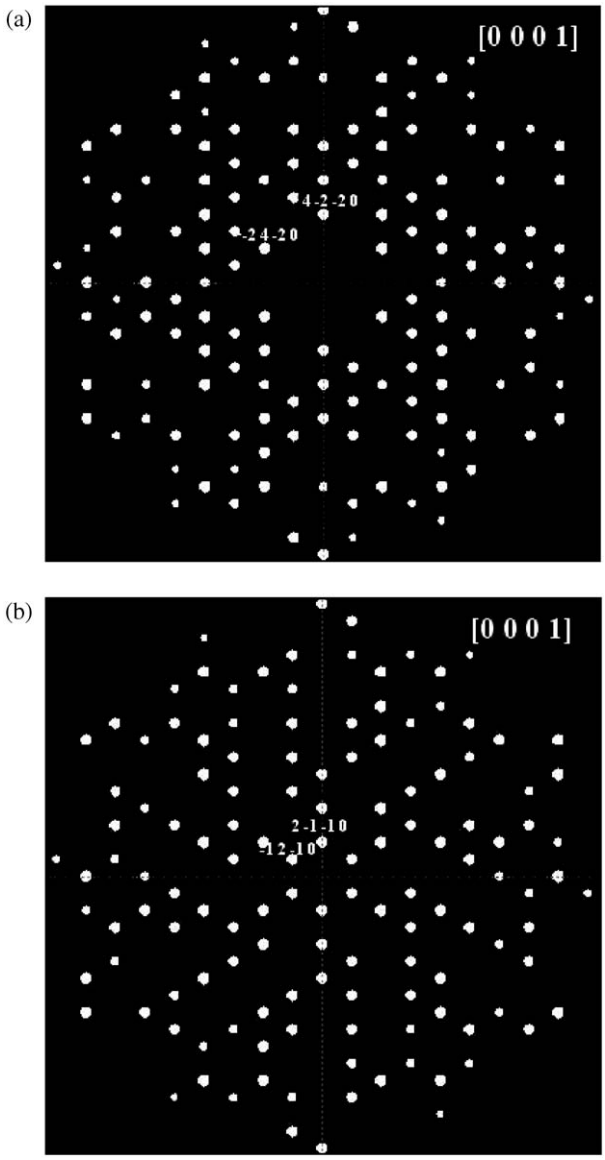

Figure 3 Electron diffraction patterns simulated on the $[0\,0\,0\,1]$ direction (a) model without OH group [22] and (b) model with OH group [24].

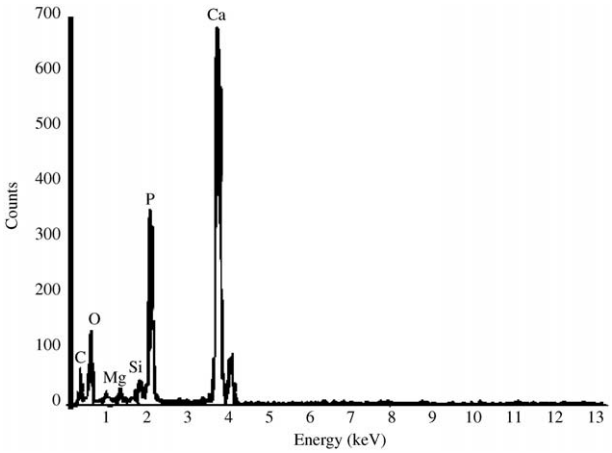

Figure 4 Typical X-ray energy dispersive spectrum (EDS) obtained from the morphologies of hydroxylapatite crystals.

shape were observed in the $[0\,0\,0\,1]$ direction (Fig. 2(b)). However, in the electron diffraction patterns, such as illustrated in Fig. 2(b), an important feature was noted. All the reflections have the same intensity, which were not reproduced in the electron diffraction pattern simulation. The simulated electron diffraction pattern in the $[0\,0\,0\,1]$ direction is illustrated in Fig. 3(a). This pattern was obtained using the model reported for the hydroxylapatite structure [22]. The absence of several reflections in the electron diffraction pattern can be clearly observed in the $[0\,0\,0\,1]$ direction, which are forbidden reflections for the CaHAP structure. However, the experimental electron diffraction pattern shows the presence of these reflections and the analysis corresponds to the hydroxylapatite. In addition, it is important to mention that another model for CaHAP structure was found [24]. The difference among them is the hydroxyl (OH) group presence on the structure. Also the electron diffraction pattern simulated with this model was obtained and it is illustrated in Fig. 3(b). Reflections of the $\{2\,-1\,-1\,0\}$ plane family can be observed in this pattern, which were not observed in the pattern illustrated in Fig. 3(a). However, the lack of some reflections can still be observed. Therefore, both CaHAP models do not reproduce the experimental pattern.

On the other hand, the chemical analysis carried out in both morphologies indicate that in addition to Ca, O, and

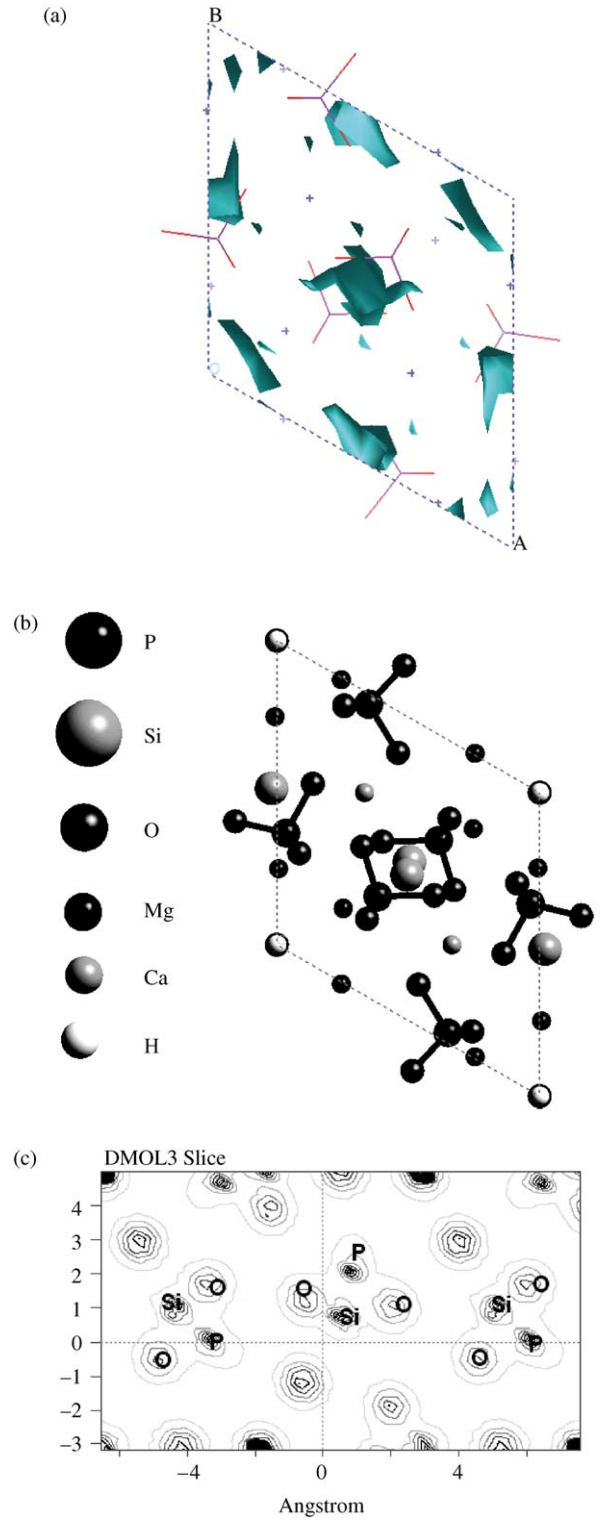

Figure 5 (a) Free volume of the hydroxylapatite unit cell, (b) hydroxylapatite crystal structure with Si and Ca atoms and OH and (c) a cross section of the electronic charge density distribution of the atoms in the CaHAP structure showing the coordination of the Si atom with two O atoms.

P, there are other chemical elements such as Si and Mg in the structure. The energy dispersive spectrum obtained from the CaHAP crystals is showed in Fig. 4, where clearly the small peak presence of Si and Mg can be observed. These chemical impurities were not considered in both simulation process and their presence in the structure does not suggest a solid solution by the obtained simulation results. For this reason, impurities of Si atoms on the CaHAP structure was introduced and some Ca

TABLE II Asymmetric unit of CaHAP with two hydroxyl groups, Si and substitution of Ca per Mg after relaxation

	Atom	*X*	*Y*	*Z*	*F*
1	Mg	2.766	4.892	−0.136	1.00
2	CA	2.199	8.404	1.573	1.00
3	P	3.332	1.781	1.577	1.00
4	O	2.783	3.217	1.591	1.00
5	O	4.875	1.777	1.500	1.00
6	O	2.809	0.996	0.374	1.00
7	O	0.042	0.237	1.396	1.00
8	H	−0.005	0.229	0.455	1.00
9	Si	1.832	0.817	3.245	1.00
10	O	1.363	2.418	3.561	1.00
11	H	1.863	3.016	3.036	1.00

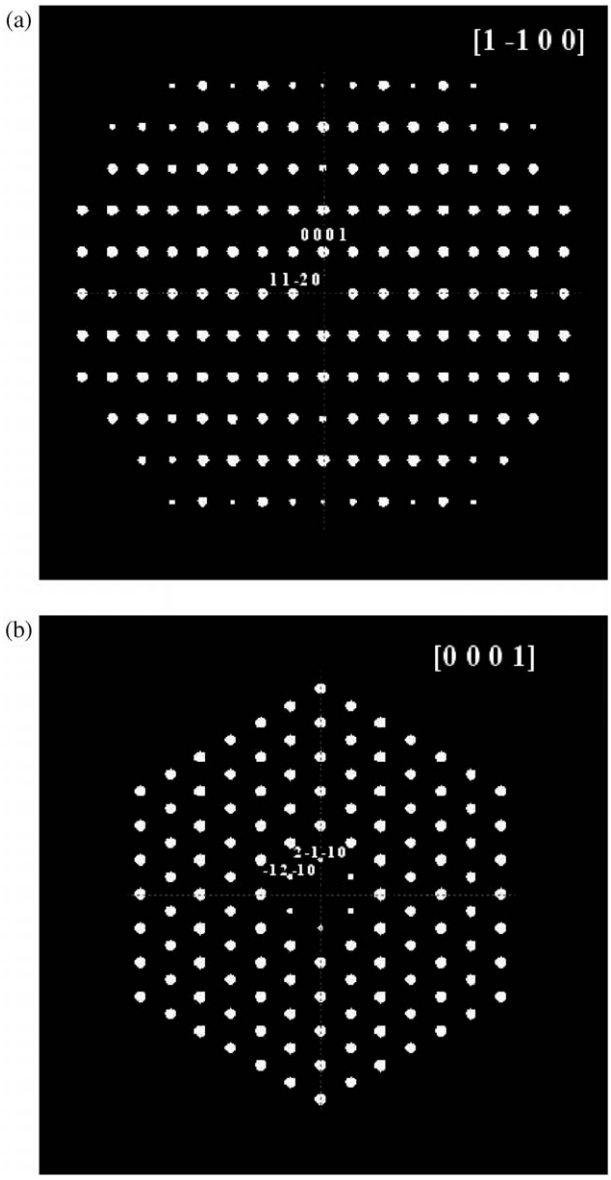

Figure 6 Electron diffraction pattern obtained by simulation of the model of Fig. 5(b). (a) [1 −1 0 0] and (b) [0 0 0 1] directions.

atoms were substituted by Mg atom according to the literature [25] in the CaHAP model, which have OH groups.

The free volume of the hydroxylapatite unit cell was calculated by Cerius2 program. The total volume for CaHAP unit cell was 529 Å^3/u.c. and free volume was 28.18 Å^3/u.c. Fig. 5(a) shows the free volume of the unit

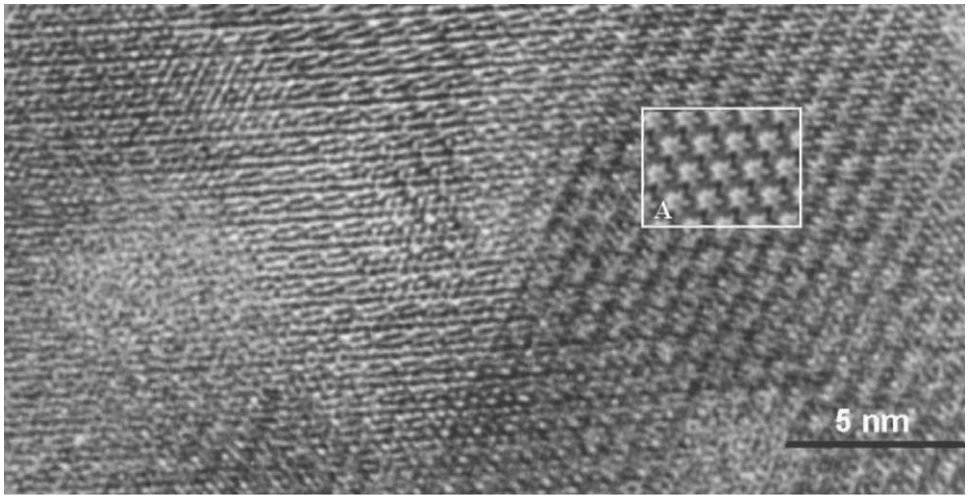

Figure 7 Experimental HRTEM image. Inset A shows simulated image over experimental image.

cell where the Si atom and hydroxyl group were introduced.

Subsequently the geometric optimization of the structure with the introduction of these atoms was calculated by Fast-structure from Cerius2 program. This process works in such a way that the geometry of the system is optimized and the energy or the system was calculated. The initial energy for the CaHAP model was $-19\,095.02$ eV and the final energy was $-19\,107.72$ eV. The energy minimization process located the Si atoms, Mg atoms, and hydroxyl groups in a position of minimum energy and the free volume was $0\,\text{Å}^3$/u.c. They finally have a split of approximately 0.2 Å and the lattice parameter of the hydroxylapatite did not showed changes. The final positions of the atoms in the asymmetric unit are illustrated in the Table II, and Fig. 5(b) shows the final structure for CaHAP in their basal state with impurities of Si atoms and substitutions of Mg atoms. The Si atom is coordinated with two oxygen atoms of the PO_4^{-3} ion. This is illustrated in Fig. 5(c) where a cross section of the electronic charge density distribution of the atoms in the structure is shown. Subsequently, a superstructure was built according to the experimental chemical composition.

Electron diffraction patterns simulated were obtained with this model along the $[1\,-1\,0\,0]$ and $[0\,0\,0\,1]$ directions. They are illustrated in Fig. 6, respectively. As can be observed, the patterns show the forbidden reflections, which were not observed in the initial models proposed for hydroxylapatite. Now these patterns are similar to the experimental electron diffraction pattern shown in Fig. 2. All reflections can be observed with the same intensity in the $[0\,0\,0\,1]$ direction, which is similar to Fig. 2(b). Also, high-resolution transmission electron microscopy (HRTEM) experimental and simulated images were obtained and these are illustrated in Fig. 7. The experimental HRTEM image corresponds to the morphology with hexagonal plane shape in the $[0\,0\,0\,1]$ direction. The simulated HRTEM image was obtained with the relaxed model. Clearly it can be observed that the simulated image (inset A) also reproduces, the experimental image. A simulated X-ray diffraction spectrum from this model was obtained, which was compared with the experimental and simulated (model according to literature [24]) X-ray diffraction spectrums. These are illustrated in Fig. 8 and the peak presence at 10.84° and 21.78° is clearly observed in the simulated spectrum with impurities (Fig. 8(c)). This spectrum reproduces the experimental spectrum, unlike the spectrum obtained by a simulation according to the model of the literature [24]. These peaks correspond to the $\{2\,-1\,-1\,0\}$ and $\{4\,-2\,-2\,0\}$ planes, respectively, and were the plane families observed in the experimental electron diffraction pattern of Fig. 2(b).

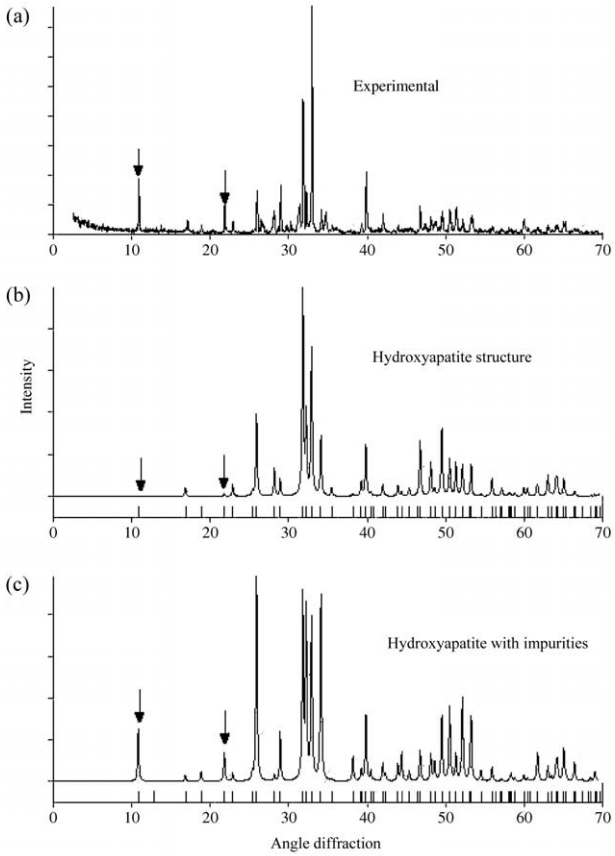

Figure 8 X-ray diffraction spectrum (a) experimental, (b) simulated with hydroxylapatite unit cell [24] and (c) obtained with the model of Fig. 5(b).

Conclusions

The presence of extraneous elements such as Si, Mg and the number of OH groups were found in both morphology types of CaHAP crystals. According to the model simulated from the CaHAP structure with these atoms we found that these elements are within the CaHAP crystal structure and their presence into the lattice did not modify the lattice parameters of the hydroxylapatite unit cell. However, they have an effect in the electron diffraction phenomena by producing forbidden reflections due to the position of the Si atoms within the crystalline structure. This phenomenon was also observed in the experimental X-ray diffraction spectrum and was reproduced by this new model.

Acknowledgments

The authors are indebted to CONACYT and VIEP-SEP for support through the projects ''Desarrollo de Materiales Cerámicos para Aplicaciones Biomédicas'' 32605-U and ''Síntesis, Caracterización y aplicación de hidroxiapatita obtenida a partir de precursores alternativos mediante los métodos hidrotermal y sólido-sólido'' III36G02.

References

1. V. RODRIGUEZ-LUGO, J. A. ASCENCIO, C. ANGELES-CHAVEZ, A. CAMACHO-BRAGADO and V. M. CASTAÑO, *Mater. Tech.* **16** (2001) 97.
2. M. GONZALEZ, J. A. BANDERAS, V. RODRIGUEZ-LUGO and V. M. CASTAÑO-MENESES, *J. Dentist.* **27** (2000) 595.
3. V. RODRIGUEZ-LUGO, G. A. CAMACHO-BRAGADO, C. ANGELES-CHAVEZ, R. CRUZ-COLIN and V. M. CASTAÑO-MENESES, in Proceedings of the 5th Interamerican Electron Microscopy Congress, Materials\Works\95.htm, 1999.
4. J. ASCENCIO-GUTIERREZ, V. RODRIGUEZ-LUGO, C. ANGELES, T. SANTAMARIA and V. M. CASTAÑO, *Comput. Mater. Sci.* **25** (2002) 413.
5. L. YUBAO, C. P. A. T. KLEIN, J. DE WIJN and S. VAN DE MEER, *J. Mater. Sci.: Mater. Med.* **5** (1994) 263.
6. T. SUGIMOTO, *Surfactant Science Series, Fine Particles, Metal Phosphate and Apatites* **92** (2000) 362.
7. J. L. NICOLOPOULOS, M. GONZALES-CALBET, M. P. ALONSO, M. T. GUTIERREZ-RIOS, M. I. DE FRUTOS and M. VALLET-REGI, *J. Solid State Chem.* **116** (1995) 265.
8. A. BIGI, L. CAMPOSTELLA, A. M. FICHERA, E. FORESTI, M. GAZZANO, A. RIPAMONTI and N. ROVERI, *J. Inorg. Biochem.* **34** (1988) 75.
9. S. V. CHIRANJEERVIRAO, J. HEEMMERLE, J. C. VOEGEL and R. M. FRANK, *Inorg. Chim. Acta* **67** (1982) 183.
10. R. Z. LEGEROS in ''Hydroxyapatite and related materials'', edited by P. W. Brown, B. Constantz (CRC Press, Boca Raton, 1994).
11. A. S. POSNER, *Physiol. Rev.* **49** (1969) 760.
12. J. C. EANES, *J. Dent. Res.* **58** (1973) 829.
13. H. FLEISCH and S. BISAZ, *Amer. J. Physiol.* **203** (1962) 671.
14. D. WALSH, J. L. KINGSTON, B. R. HEYWOOD and S. MANN, *J. Cryst. Growth* **133** (1993) 12.
15. P. G. KOUTSOUKOS and G. H. NANCOLLAS, *ibid.* **55** (1981) 369.
16. M. OKAZAKI, *Biomaterials* **13** (1992) 749.
17. R. Z. LEGEROS, J. P. LEGEROS, O. R. TRAUTZ and W. P. SLURRA, *Ad. X-Ray Anal.* **14** (1971) 57.
18. G. H. NANCOLLAS and P. G. KOUTSOUKOS, *Colloids Surface* **17** (1986) 361.
19. G. H. NANCOLLAS and P. G. KOUTSOUKOS, *J. Amer. Chem. Soc.* **85** (1981) 2403.
20. Cerius2 ''Quantum Mechanics'', April (Molecular Simulation Inc., San Diego, CA, 1997).
21. J. M. COWLEY, *Acta Crystallogr.* **12** (1959) 367.
22. A. S. PONER, A. PERLOFF and A. F. DIORIO, *ibid.* **11** (1958) 308.
23. C. ANGELES-CH, M. E. FERNANDEZ and V. RODRIGUEZ-LUGO, *Acta Microscopica* **October** (2001) 94.
24. W. E. BROWN, J. P. SMITH, J. R. LEHR and A. W. FRAZIER, *Nature* **196** (1962) 1048.
25. F. ABBONA and A. BARONNET, *J. Crystal Growth* **165** (1996) 98.

Received 4 December 2002
and accepted 16 June 2003